remote sensing

MDPI

Article

Spatial Prediction of Fluvial Flood in High-Frequency Tropical Cyclone Area Using TensorFlow 1D-Convolution Neural Networks and Geospatial Data

Nguyen Gia Trong [1,2], Pham Ngoc Quang [1,2], Nguyen Van Cuong [3], Hong Anh Le [4], Hoang Long Nguyen [5] and Dieu Tien Bui [6,*]

1 Department of Geodesy, Faculty of Geomatics and Land Administration, Hanoi University of Mining and Geology, Duc Thang, Bac Tu Liem, Hanoi 10000, Vietnam; nguyengiatrong@humg.edu.vn (N.G.T.)
2 Geodesy and Environment Research Group, Hanoi University of Mining and Geology, Duc Thang, Bac Tu Liem, Hanoi 10000, Vietnam
3 The Vietnam Agency of Seas and Islands, Nguyen Chi Thanh, Dong Da, Hanoi 10000, Vietnam
4 Department of Computer Science, Faculty of Information Technology, Hanoi University of Mining and Geology, Duc Thang, Bac Tu Liem, Hanoi 10000, Vietnam
5 Department of Geoinformatics, Faculty of Information Technology, Hanoi University of Mining and Geology, Duc Thang, Bac Tu Liem, Hanoi 10000, Vietnam
6 GIS Group, Department of Business and IT, University of South-Eastern Norway, Gullbringvegen 36, N-3800 Bø, Norway
* Correspondence: dieu.t.bui@usn.no

Abstract: Fluvial floods endure as one of the most catastrophic weather-induced disasters worldwide, leading to numerous fatalities each year and significantly impacting socio-economic development and the environment. Hence, the research and development of new methods and algorithms focused on improving fluvial flood prediction and devising robust flood management strategies are essential. This study explores and assesses the potential application of 1D-Convolution Neural Networks (1D-CNN) for spatial prediction of fluvial flood in the Quang Nam province, a high-frequency tropical cyclone area in central Vietnam. To this end, a geospatial database with 4156 fluvial flood locations and 12 flood indicators was considered. The ADAM algorithm and the MSE loss function were used to train the 1D-CNN model, whereas popular performance metrics, such as Accuracy (Acc), Kappa, and AUC, were used to measure the performance. The results indicated remarkable performance by the 1D-CNN model, achieving high prediction accuracy with metrics such as Acc = 90.7%, Kappa = 0.814, and AUC = 0.963. Notably, the proposed 1D-CNN model outperformed benchmark models, including DeepNN, SVM, and LR. This achievement underscores the promise and innovation brought by 1D-CNN in the realm of susceptibility mapping for fluvial floods.

Keywords: fluvial flood; 1D-CNN; deep neural networks; geospatial data; tropical areas

Citation: Trong, N.G.; Quang, P.N.; Cuong, N.V.; Le, H.A.; Nguyen, H.L.; Tien Bui, D. Spatial Prediction of Fluvial Flood in High-Frequency Tropical Cyclone Area Using TensorFlow 1D-Convolution Neural Networks and Geospatial Data. *Remote Sens.* **2023**, *15*, 5429. https://doi.org/10.3390/rs15225429

Academic Editor: Raffaele Albano

Received: 2 October 2023
Revised: 4 November 2023
Accepted: 10 November 2023
Published: 20 November 2023

1. Introduction

Floods persist as one of the most destructive natural disasters globally, plaguing communities across the globe and posing significant threats to both life and property. Over the last two decades (1989–2017), floods have impacted over 45% of the world's population, resulting in 142,088 deaths and losses totaling $656 billion [1]. Recent studies [2–4] underscore the increasing gravity of the flood issue in the foreseeable future, primarily due to the adverse impacts of global warming and climate change. These factors are expected to amplify extreme rainfall events worldwide, resulting in a higher frequency and intensity of floods. Floods can be categorized into various types based on their water sources, encompassing coastal floods, urban floods, dam-break floods, flash floods, and fluvial floods [5]. Among them, fluvial floods, where overflowing rivers inundate adjacent lands, are one of the most prevalent and devastating types [6]. Hence, dedicating resources to research and

innovation aimed at enhancing fluvial flood prediction techniques, which are essential for formulating resilient flood management strategies, is crucial.

Literature reviews indicate that studies on fluvial floods from a hazard perspective are typically conducted using various approaches across different branches of research [7]. Scholars and experts in fields such as hydrology, climatology, geology, geography, and environmental science have explored the complexities of fluvial floods, each offering unique insights and methodologies. These multidisciplinary approaches encompass a wide range of techniques, from field studies to advanced modeling and data analysis, and broadly, flood prediction models can be classified into the rainfall-runoff group [8] and the 'on/off' classification group [9]. The rainfall-runoff group relies on well-known empirical models, such as the SCS-Curve Number model [10], as well as physical-based models like TOPMODEL [11] and SWAT [12]. These models have demonstrated their efficiency in predicting both spatial and temporal scales with remarkable accuracy. However, it is essential to note that these models demand long-term monitoring data series for reliable predictive outcomes [13]. Therefore, newer methods, specifically those falling under the 'on/off' classification approach, have been considered.

Models in the 'on/off' classification group do not require extensive time series data; instead, they offer spatial predictions of floods [14]. These models utilize input data from historical flood events and conditioning factors from relevant studies, field surveys, and optical or radar imagery interpretations obtained through remote sensing techniques. In this context, machine learning emerges as a pivotal tool for characterizing flood susceptibility areas, yielding promising results, i.e., support vector machines [15], random forests [16], Gaussian Mixture model [14], decision Trees [17], neural networks [18], neural fuzzy [19], and regression splines [20]. In general, these machine learning models offer high prediction accuracy for floods owing to their proficiency in discerning intricate patterns within extensive and varied spatial datasets. These models can uncover nuanced relationships that might pose challenges for conventional methods by analyzing historical flood data in conjunction with diverse geo-environmental indicators. Nevertheless, to date, no universal method or technique has been identified as the best for all regions. Therefore, ongoing research to explore new algorithmic models for flood forecasting remains imperative.

In more recent years, with the development of information technology, deep learning has surfaced as a powerful method for flood susceptibility mapping, presenting substantial potential to improve our understanding and management of regions prone to flooding, including deep neural networks [21,22], LSTM neural networks [23], 1D- Convolution Neural Networks (CNN) [24,25], 2D-CNN [25,26], 3D-CNN [27], U-Net, and WU-Net [28]. While these models have the capacity to enhance the accuracy of flood predictions, further research is necessary to expand the knowledge base, particularly in terms of achieving more reliable conclusions compared with traditional machine learning methods.

This study endeavors to partially fill a gap in the existing literature by investigating the potential application of 1D-CNN for spatial predictions of fluvial floods in Quang Nam, a province in central Vietnam that is frequently affected by tropical cyclones. In this province, significant rainfall events are commonplace; these are often intensified by tropical storms, resulting in occurrences of flooding and landslides [29]. In this study, we pay specific attention to events within the last five years. In 2022 alone, as documented in the report by the Quang Nam Steering Committee for Natural Disaster Prevention and Search and Rescue, from October 13 to 15, 2022, the region experienced an extensive period of intense rainfall, with precipitation levels ranging from 250 to 350 mm. These torrential rains resulted in severe flooding across the province, causing six deaths. A total of 2695 residences were inundated to a depth of less than 1 m, while 1423 homes were submerged at depths between 1 and 3 m.

2. Materials and Methods

2.1. Study Area and Data

2.1.1. Study Area

The research area encompasses Quang Nam province, situated within the central coastal region of Vietnam and spanning an area of 3173.4 square kilometers. Geographically, it extends from 14°56′ to 16°04′ north latitude and from 107°11′ to 108°44′ east longitude (Figure 1). The topography is diverse and ranges from coastal areas with sandy beaches to rugged mountains, fertile plains, and river valleys. The elevation ranges from 0 to 2594.1 m a.s.l, with the mean and the standard deviation at 466.9 m and 405.5 m, respectively. The Truong Son range dominates the western part of the province [30], a mountainous region that runs parallel to the coast. Rugged terrain, dense forests, and high peaks characterize this region.

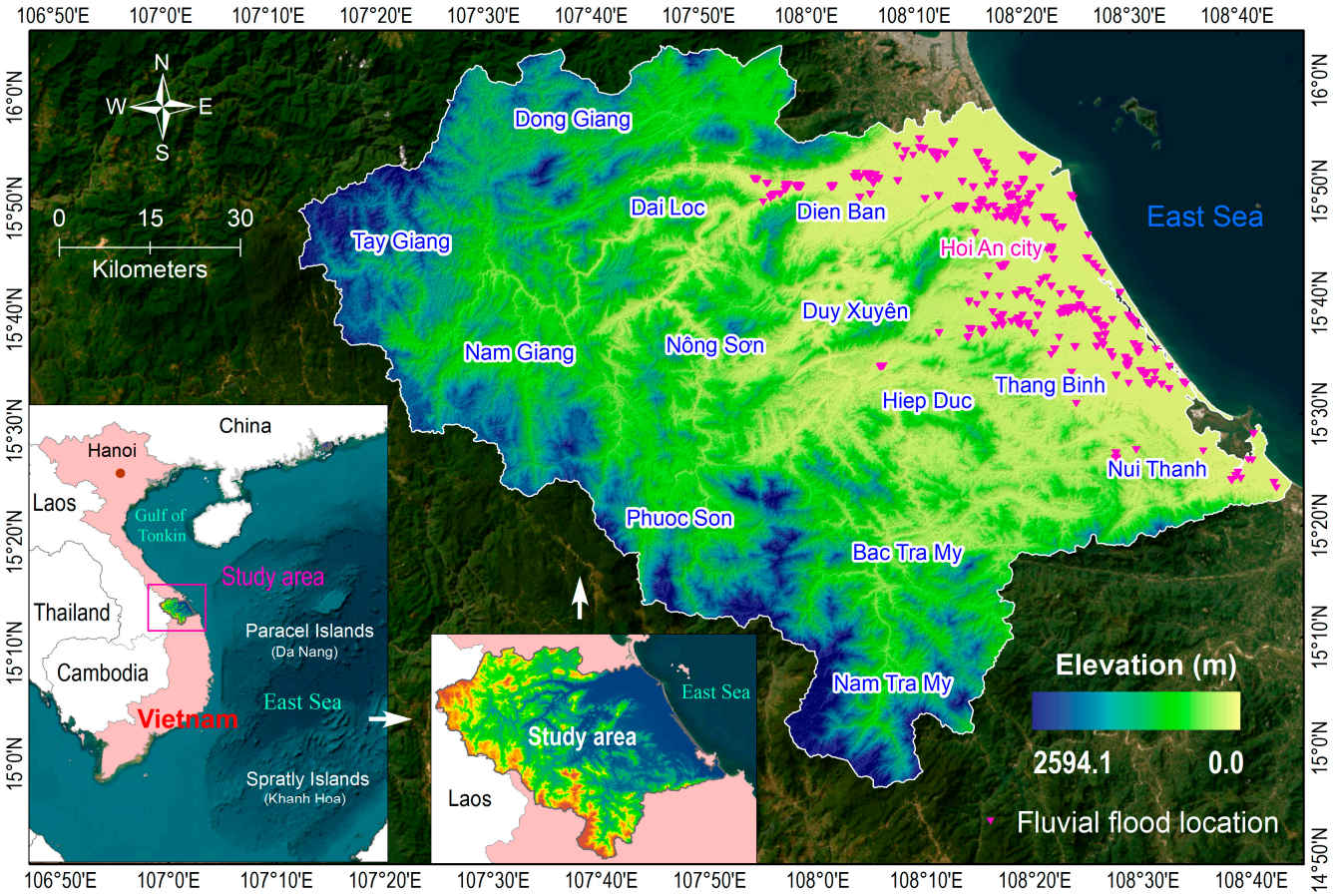

Figure 1. Location of the Quang Nam province and fluvial flood inventories.

In contrast to the mountainous western region, the eastern part of the province, especially around the city of Tam Ky and the coastal areas, consists of fertile plains and lowlands. The province exhibits a range of slopes, spanning from 0 to 82.7 degrees. Specifically, regions with slopes between 0 and 3 degrees constitute 14.7% of the total area, while those with slopes ranging from 3 to 7 degrees comprise 10.1%. Approximately 20% of the study area features slopes between 7 and 15 degrees, with the majority, i.e., accounting for 46.1% of the study area, exhibiting slopes falling within the range of 15 to 35 degrees.

From a hydrological perspective, Quang Nam province is home to a large river network with a significant flow rate, ensuring a stable water supply all year round. The Vu Gia and Thu Bon Rivers stand out, with a basin area of about 10,350 km^2 [31,32], and are an essential source of water in the region. Additionally, other significant river systems, including the Tam Ky, Cu De, Tuy Loan, and Ly Li rivers, contribute to the hydrological richness of

the region, with a combined basin area exceeding 1800 km^2. These rivers maintain high flow rates and serve as perennial water sources, making them immensely valuable for hydroelectric power generation, transportation, and irrigation in the province.

In terms of geology, more than 20 formations and complexes are recognized, and their distributions are different. Eight lithological units, i.e., quaternary, the A Vuong Formation, the Kham Duc Formation, the Tac Po Formation, the Ben Giang Complex, the Nong Son Formation, the Song Bung Formation, and the Chu Lai Complex, cover 70.78% of the total study area. The main lithologies are sericite-quartz schist, quarzitic sandstone, feldspar-hornblende schist, sandy clay, biotite gneiss, gabbro diorite, pebble conglomerate mixed with sandstone, conglomerate, and granite gneiss (Table 1).

Table 1. Lithology of the Quang Nam province.

No	Lithological Unit	Area (%)	Main Lithology
1	A Vuong formation	16.76	Sericite—quartz schist, quartzitic sandstone, micaceous schist,
2	Kham Duc formation	15.49	Feldspar-hornblende schist, two-mica garnet schist, biotite schist
3	Quaternary	11.61	Sandy clay, clay sand, gravel, pebbles, and grit
4	Tac Po formation	7.92	Biotite gneiss, biotite plagiogneiss, graphite-bearing schist
5	Ben Giang complex	7.39	Gabbrodiorite, diorite, and hornblende-biotite granite
6	Nong Son formation	6.74	Pebble conglomerate mixed with sandstone, conglomerate, gravel
7	Song Bung formation	4.86	Conglomerate, claystone, siltstone, and gravestone
8	Chu Lai complex	3.81	Granitic gneiss, migmatite granite, and garnet-biotite granite
9	Dai Loc complex	3.34	Gneissogranite of marginal facies and granite
10	Nui Vu formation	3.17	Plagioclase-amphibole schist, quartz-mica schist, and cherty schist
11	Hai Van complex	3.00	Biotite granite, two-mica granite, and granite aplite
12	Ban Co formation	1.91	Gritstone, conglomerate, and pebble-bearing gritstone
13	Ba Na complex	1.14	Biotite granite and two-mica granite
14	Song Re formation	1.11	Biotite-hornblende gneiss and plagiogneiss and biotite gneiss
15	Tra Bong complex	1.00	Diorite, quartz-diorite, granodiorite, tonalite, granite
16	Long Dai formation	0.67	Quartz siltstone, sandstone, clay shale, silty sandstone
17	Khe Ren formation	0.65	Siltstone, small-grained sandstone, siltstone, sandstone
18	Nui Ngoc complex	0.43	Gabbro and gabbrodiabase
19	Huu Chanh formation	0.29	Chocolate siltstone interbeds of sandstone
20	Others	8.70	Diorite, quartz diorite, Gabbroamphibolite, and serpentinized

Quang Nam lies within a tropical climate zone [33] featuring a distinct duality of seasons, i.e., the wet and dry seasons, both influenced by the cold northern winter. The wet season typically extends from October through December, while the dry season spans from February to August. January and September are transitional months, marked by fluctuating weather conditions and substantial precipitation. The annual average temperature hovers around 25.6 °C, with the delta occasionally experiencing temperatures dipping below 12 °C during winter. Air humidity averages approximately 84%, and the region receives an average annual rainfall ranging from 2000 to 2500 mm [34].

2.1.2. Flood Inventory Map

Given that areas prone to flooding have experienced such incidents in both the past and present, and recognizing that these indicators serve as essential data for the development of predictive models, it becomes imperative to establish flood inventories and identify pertinent indicators [14]. In this project, we extracted data from a total of 4156 flood occurrences over the past five years, sourced from Project No-03/HD-KHCN-NTM 2022, which received funding from the Ministry of Natural Resources and Environment in Vietnam.

Accordingly, Sentinel-1 SAR imagery, combined with a change detection method [18,35], was used to detect fluvial flood locations. It is worth mentioning that the Sentinel-1 mission represents a prominent constellation of C-band Synthetic Aperture Radar (SAR) satellites [36], consisting of two polar-orbiting spacecraft. Each satellite is outfitted with a C-band SAR sensor capable of acquiring imagery with a spatial resolution of 10 m. This configuration ensures a frequent revisit rate, guaranteeing the availability of imagery every six days when operating in constellation mode. A total of six Sentinel-1 SAR images from 2018–2022 were used for fluvial flood detection in Quang Nam province (Table 2). Figure 2 illustrates a methodological flow chart for detecting flood areas using multi-temporal Sentinel-1 SAR images.

Table 2. Sentinel-1 SAR images used for fluvial flood detection in Quang Nam province.

No	Acquisition Date	Mode	Polarization Used	Relative Orbit	Direction	Note
1	3 December 2018	IW	VV	120	Descending	Pre-event
2	11 December 2018	IW	VV	55	Ascending	Post-event
3	1 October 2020	IW	VV	55	Ascending	Pre-event
4	13 October 2020	IW	VV	55	Ascending	Post-event
5	8 October 2021	IW	VV	55	Ascending	Pre-event
6	12 October 2021	IW	VV	120	Descending	Post-event

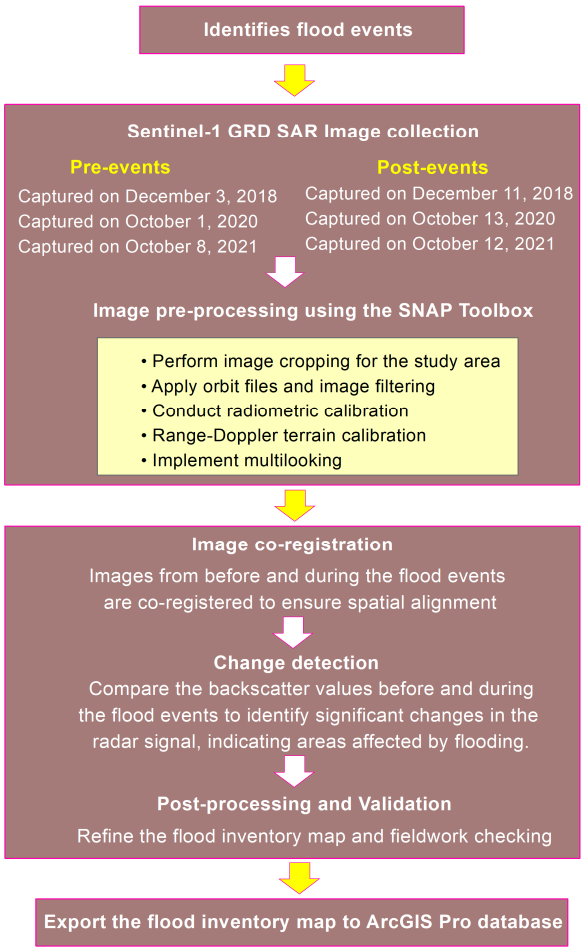

Figure 2. Methodological flow chart for detecting flood areas in this research.

As shown in Table 2 and Figure 2, three pairs of Sentinel-1 SAR images were collected before and after flood events. These images capture radar backscatter values which can be used to detect landscape changes. The SAR images undergo pre-processing steps, including cropping for the study area, applying orbit files, image filtering, radiometric calibration, Range-Doppler terrain calibration, and multilooking, ensuring standardization for analysis. Following the co-registration of pre-flood and flood images for spatial alignment, a change detection technique was applied to identify affected areas. Subsequently, flood areas were refined and validated through fieldwork checks. Finally, these flood areas were exported to the ArcGIS Pro database.

2.1.3. Flood Indicators

The determination of flood indicators is crucial for flood modeling and prediction; therefore, in this study, based on a literature review, including [21,37–41], and our analysis of the flood locations and of the geo-environmental conditions of the study areas, a total of 12 flood indicators were considered: elevation, slope, aspect, relief amplitude, topographic wetness index (TWI), stream density, geology, landuse/landcover (LULC), soil type, Normalized Difference Vegetation Index (NDVI), Normalized Difference Water Index (NDWI), and rainfall.

First, a digital elevation model (DEM) for the Quang Nam province was derived from the ALOS DEM with a spatial resolution of 30 m. The DEM is provided by the EORS of JAXA and is available at www.eorc.jaxa.jp. Using the DEM, the elevation, slope, aspect, curvature, relief amplitude, and TWI were obtained. Elevation was chosen as it aids in discerning the inherent water flow patterns during a flood event. This is because water naturally moves in the direction of lower elevation, driven by gravity [42]. When water encounters elevated terrain, it proceeds from higher elevations to lower ones. As depicted in Figure 3a, the elevation within the study area exhibits considerable variation, spanning from 0.0 to 2594.1 m. Notably, regions of elevated terrain are predominantly situated in the northwest and southwest, while lower-lying areas are primarily found in the eastern regions; these are particularly susceptible to frequent flash flood events.

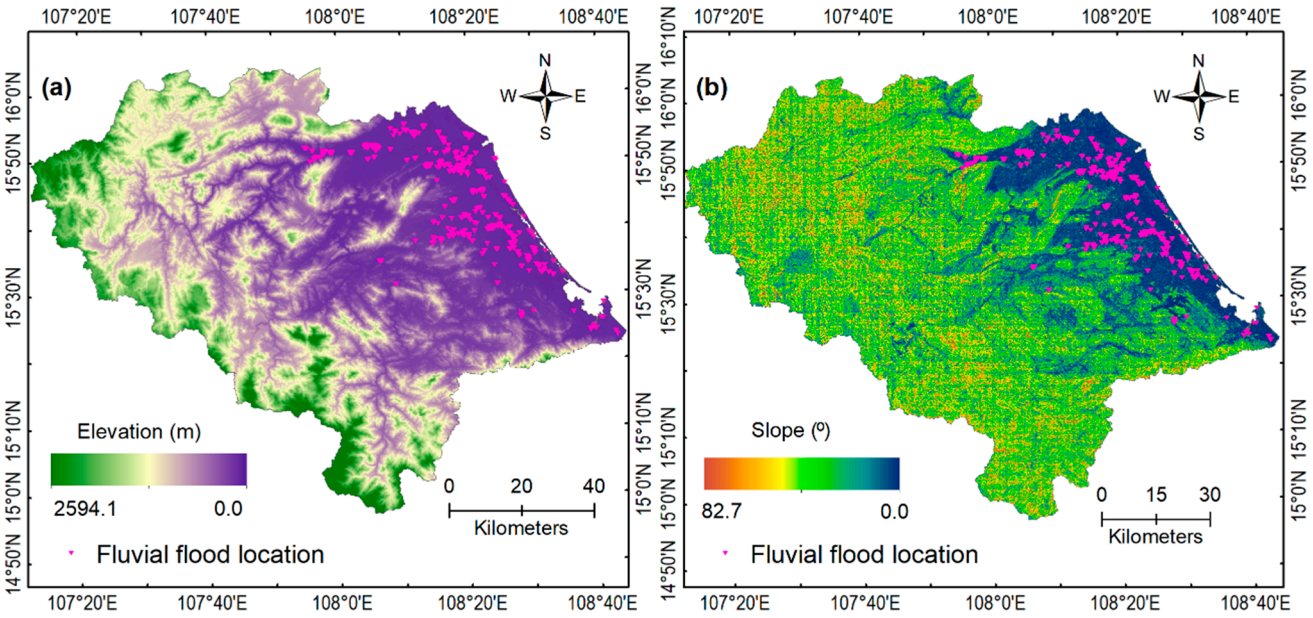

Figure 3. *Cont.*

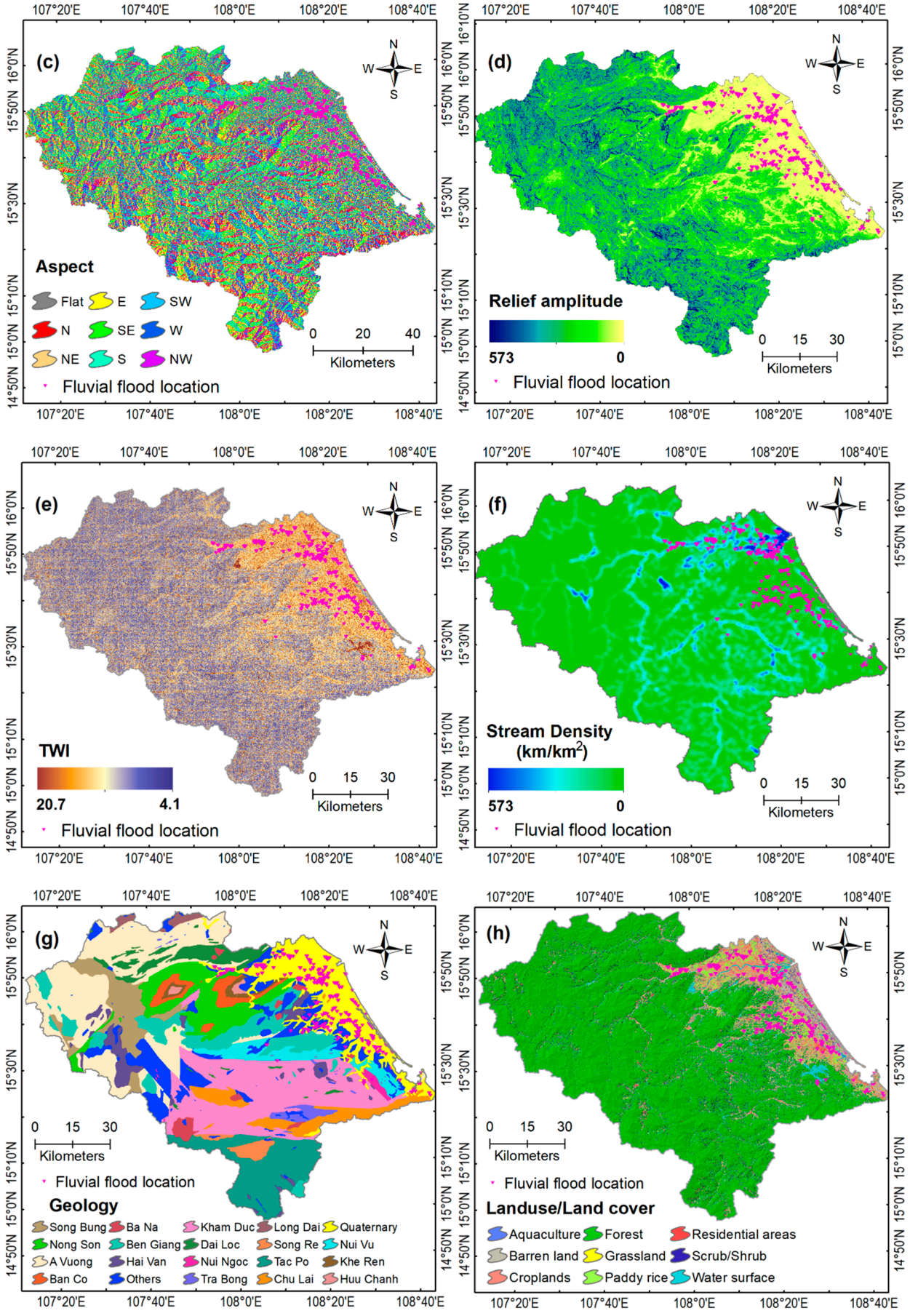

Figure 3. *Cont.*

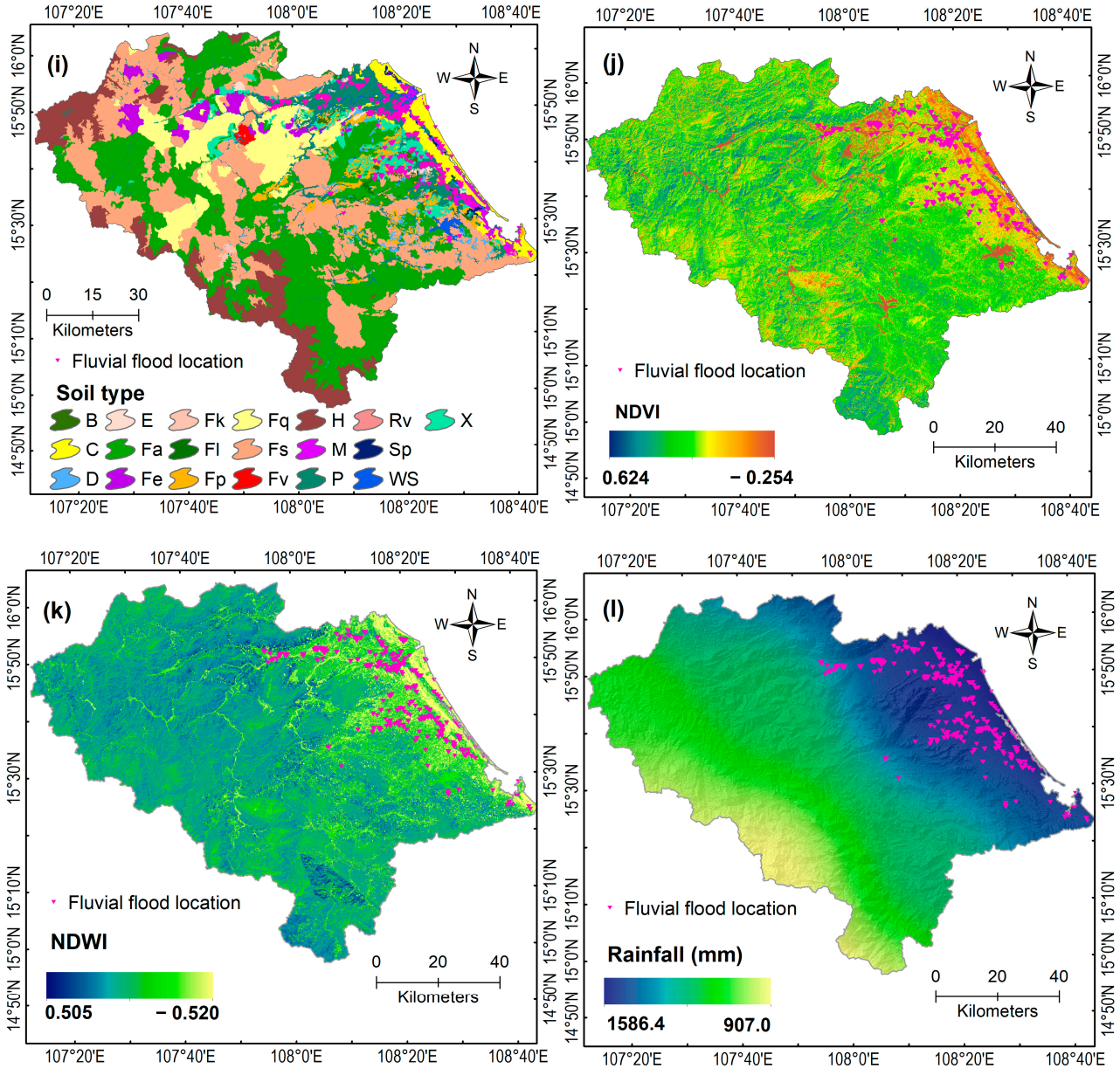

Figure 3. Flood indicator: (**a**) Elevation, (**b**) Slope, (**c**) Aspect, (**d**) Relief amplitude, (**e**) TWI, (**f**) Stream density (**g**) Geology, (**h**) Landuse/Landcover (LULC), (**i**) Soil type, (**j**) NDVI, (**k**) NDWI, and (**l**) Rainfall.

Slope (Figure 3b) is an important indicator that influences how water moves across the landscape and can exacerbate or mitigate flood hazards [43,44]. In this regard, a region with significant slope can diminish infiltration and elevate runoff, whereas a region with a gentler slope can decelerate the flow velocity. Aspect refers to a slope's compass direction, such as north, south, east, or west. Aspect is an essential indicator for flood modeling because it significantly affects rainfall distribution [45]. An aspect map of the study area with nine classes is shown in Figure 3c. Relief amplitude is a valuable parameter in flood modeling because it directly affects the velocity of water flow [46], i.e., water flows from higher elevations to lower elevations due to gravity; the steeper the relief, the faster the water will flow as it moves downhill. The relief amplitude for the study area, which is shown in Figure 3d, was computed from the DEM using the focal statistics tool in ArcGIS Pro. The TWI (Figure 3e) indicator was chosen for flood modeling in this analysis because it utilizes topographic data to provide valuable insights into the moisture levels and drainage

patterns within a landscape [47], essential factors for comprehending and forecasting flooding events.

Regarding stream density, this indicator reflects the extent of drainage network development and is widely acknowledged as the primary factor influencing flow processes within a watershed [48]. In this research, the stream network for the Quang Nam province was extracted from the Open Street Map (www.openstreetmap.org) and was then used to compute the stream density map (Figure 3f) using the Line Density tool in ArcGIS Pro. The stream density ranged from 0.0 to 16.1 km/km^2, with high river densities in the northeast of the study area.

Geology was incorporated into this analysis due to its impact on drainage characteristics, channel formation, and capacity for water conveyance [49,50]. This is because various rock types and geological formations can either facilitate or impede water flow. This study generated a geological map (Figure 3g) using a categorization scheme comprising 20 distinct classes. The source data for this map were derived from the Geological and Mineral Resources Maps [51], available at a scale of 1:200,000, as provided by the Ministry of Natural Resources and Environment of Vietnam.

LULC should be selected for flood modeling because it has substantial impacts on infiltration and runoff generation [12,52]. In this regard, land use and land cover characteristics directly affect the ability of an area to absorb rainfall or allow it to flow over the surface, which relates to flooding. In this study, a LULC map depicting 12 distinct categories for the Quang Nam province (see Figure 3h) was generated. This map was assembled using a 30-m resolution LULC dataset from the year 2020, sourced from the Japan Aerospace Exploration Agency (JAXA) and available at www.eorc.jaxa.jp (accessed on 10 May 2023).

Soil type is a crucial parameter in flood modeling due to its direct relevance to infiltration patterns and runoff processes, which are fundamental factors in flood dynamics [53]. According to Zhan and Ng [54], different soil types exhibit varying degrees of permeability, influencing the speed at which water can either infiltrate into the ground or flow over the surface. The soil type map utilized in this study consisted of 18 distinct categories, as depicted in Figure 3i. The soil type data were sourced from national pedology maps at a 1:100,000 scale, which were provided by the Ministry of Agriculture and Rural Development of Vietnam.

NDVI and NDWI, two remote sensing indices, were included in this analysis because they serve as proxies for the vegetation and water content, both of which are pertinent indicators in flood assessments. NDVI values correspond to the condition and thickness of vegetation in the study area. Regions featuring lush and robust plant cover can decelerate surface runoff by encouraging water absorption and mitigating erosion; conversely, areas with scant or deteriorated vegetation are prone to swift runoff [55]. In the case of NDWI, this indicator exhibits sensitivity to water content through the recognition of distinctive spectral signatures [56]. Consequently, its utilization has the potential to improve flood prediction accuracy. In this work, we computed the NDVI (Figure 3j) and NDWI (Figure 3k) for the study area using the reflectance values extracted from bands 4, 5, and 6 of Landsat 8 OLI (Operational Land Imager) imagery with 30 m resolution (available at www.earthexplorer.usgs.gov, accessed on 16 May 2023), using Equation (1) [57] and Equation (2) [58], below:

$$\text{NDVI} = (\text{Band 5} - \text{Band 4})/(\text{Band 5} + \text{Band 4}) \quad (1)$$

$$\text{NDWI} = (\text{Band 5} - \text{Band 6})/(\text{Band 5} + \text{Band 6}) \quad (2)$$

Rainfall plays a pivotal role in shaping the formation and dynamics of water flow within a watershed [59]. It significantly influences the volume, speed, and behavior of floodwaters, and as such, it directly impacts flooding. In this project, we employed rainfall data spanning five years, from 2017 to 2021, with a maximum of 15 days of data. This information was utilized to create a rainfall map using the Inverse Distance Weight interpolation method [60]. The rainfall data were obtained from the POWER project, National Aeronautics and Space Administration (NASA) (available at https://power.larc.

nasa.gov, accessed on 16 May 2023). A rainfall map of the study area is shown in Figure 3l. As shown, the rainfall levels in this region exhibited a range from 907.0 mm to 1586.4 mm, displaying an uneven spatial distribution.

2.2. 1D-Convolution Neural Network

Deep learning is a specialized field within machine learning that places emphasis on neural networks comprising multiple layers. It has achieved groundbreaking success in a wide range of real-world applications [61]. Within the domain of deep learning, the 1D Convolutional Neural Network (1D-CNN) has garnered attention for its ability to capture meaningful features, making it suitable for both classification and regression tasks in environmental modeling and predictions, i.e., fires [62], landslides [63], and floods [24].

In a 1D-CNN, the network structure typically consists of the input layer and one or more convolutional layers, followed by pooling layers, flattening, fully connected layers, and the output layer [64]. The purpose of the 1D-CNN in the context of fluvial flood susceptibility mapping is to build a prediction model that infers the flood indicators to output flood susceptibility indices.

- **Input layer**: the input layer is the matrix of the input flood indicators X ($X = [x_1, x_2, x_3, \ldots, x_n]$), where the output layer is the flood susceptibility (Y) with values belonging to [0, 1].
- **Convolutional layer**: The 1D-CNN applies convolutional operations to the input of a set of filters, also known as kernels. Each filter has weights (W) and biases (b). Thus, the convolution operation at a given position i can be represented as below:

The convolutional layer employs kernels and activated functions to transform the input layer into pooling layers using Equation (3), as follows:

$$y_i = f_1\left(\sum_{j=1}^{Z} W_j x_{i+j-1} + b_1\right) \quad (3)$$

where y_i is the the output at position i, z is the size of the filter, and f is the activation function used.

- **Pooling Layer**: After the convolutional layer, the pooling layer can be used to reduce the dimensionality of the feature maps.
- **Fully Connected Layer**: In this layer, each neuron in a fully connected layer is connected to every element in the flattened vector. The output from these layers can be represented as:

$$Y = f_2(Wx + b_2) \quad (4)$$

where Y represents the output, f_2 is a non-linear activation function (e.g., softmax for classification or linear for regression), W is the weights, and b_2 is the bias.

- **The output layer**: The final output is the probability belonging to the flood class.

3. Proposed Methodology for Spatial Prediction of Fluvial Inundation Using 1D-CNN

This section describes the proposed methodology for the spatial prediction of fluvial inundation using 1D-CNN. This study employed the SNAP toolbox to process Sentinel-1 SAR imagery when generating flood inventories. In contrast, ArcGIS Pro 3.0 was utilized to process flood indicators and code them for integration into the 1D-CNN model. The Python code for the 1D-CNN model can be accessed at www.tensorflow.org (accessed on 16 May 2023), while the authors developed a Python script to convert the twelve flood indicators into the input format for the 1D-CNN model and to translate the model's output into a flood susceptibility map. A flowchart of the proposed methodology is shown in Figure 4.

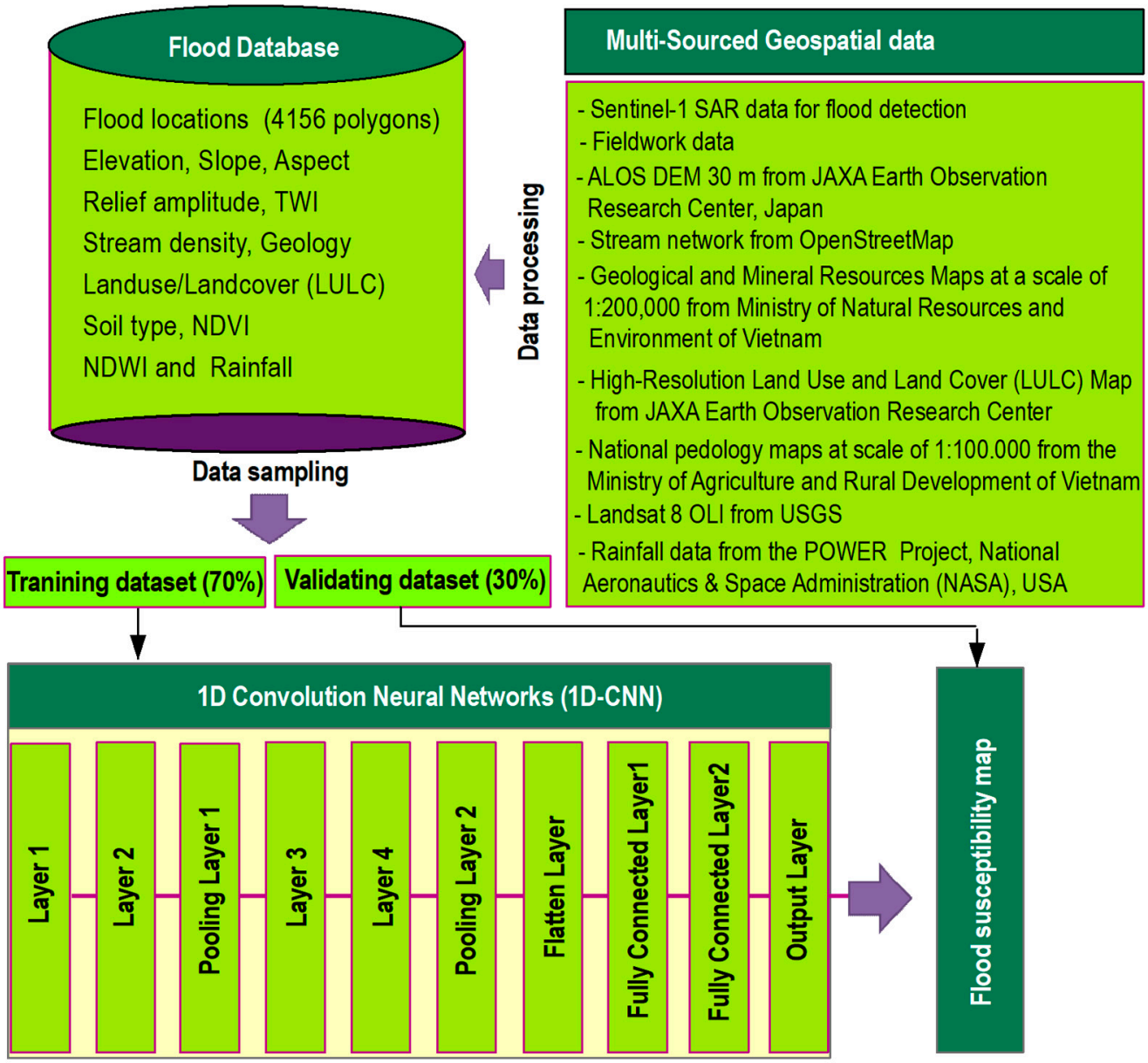

Figure 4. Flowchart of the methodology proposed in this research.

3.1. Fluvial Flood Database

In the first step, a fluvial flood database for the Quang Nam province was established using ArcGIS Pro 3.0 in the ESRI-geodatabase format [65]. Then, the reference system of WGS 84 UTM Zone 48 (Projection: Transverse Mercator, Central Meridian: 105.0, Scale Factor: 0.9996, Latitude of Origin: 0.0) for the study was specified for the database. Next, the twelve flood indicators (elevation, slope, aspect, relief amplitude, TWI, stream density, geology, LULC, soil type, NDVI, NDWI, and rainfall) and 4156 flood locations were imported into the database. All twelve flood indicators were converted into a raster format with a 30 m resolution. It should be noted that among the 12 flood indicators, aspect, geology, LULC, and soil type are categorical indicators. Therefore, a transformation process, as described in [20], was used to convert these indicators into continuous indicators.

As the 1D-CNN necessitates input data to be within the 0–1 range for improved training stability, faster convergence, and enhanced overall network performance, a normalization process was executed on the twelve flood indicators in ArcGIS Pro. This was achieved using the equation below in conjunction with the Raster Calculator tool.

$$\text{NewFI} = (\text{FI} - \text{Min(FI)} / (\text{Max(FI)} - \text{Min(FI)}) \quad (5)$$

where NewFI represents the new flood indicator value and FI denotes the original flood indicator value. Max (FI) and Min (FI) correspond to the maximum and minimum raster values among the flood factors, respectively.

Together with 4156 flood locations, an equal number of non-flood locations were randomly generated outside the flood-prone areas. Then, values of '1' and '0' were assigned for the flood and non-flood locations, respectively. Subsequently, all these locations were randomly divided into training and validation datasets, adhering to a 70:30 ratio [66]. Ultimately, a sampling procedure was executed in ArcGIS Pro to extract the values of all twelve flood indicators. Consequently, the training dataset comprised 5818 samples, while the validation dataset consisted of 2494 samples.

3.2. Feature Selection for Flood Indicators

As elaborated in Section 2, a comprehensive set of twelve flood indicators was initially considered, drawing from our literature review and analysis of flood occurrences in conjunction with the characteristics of the study area. However, the relevance of these indicators to flooding had to be quantified and ranked, and non-relevant indicators had to be eliminated. This enhanced the model's generalization, accelerated computations, and improved the interpretability of the 1D-CNN model. In this study, a correlation analysis was conducted to assess the significance of each flood indicator. This analysis measured the Pearson's correlation [67] between the flood indicator and fluvial flood occurrences.

However, the occurrence of floods can also be related to the interaction of many different indicators, so our assessment of the role of these indicators had to consider their mutual interactions. Among various feature selection methods and techniques, the wrapper has proven its efficiency [68] due to its ability to cover the interactions among all indicators in predicting floods [39]. This method evaluated all possible combinations of the twelve flood indicators, considering the Mean Absolute Error (MAE) as the evaluation criterion, as defined in Equation (6) and as suggested by [69]. Consequently, the contribution of each flood indicator was quantified by measuring its impact on MAE through an iterative and systematic greedy search process [70]. Herein, initially, the wrapper algorithm assessed the performance of the full model with 12 flood indicators measured by MAE. Subsequently, an iterative process involved exploring various combinations of these indicators through a running loop. The MAE of the resulting sub-models was then compared with that of the full model. Finally, the contribution of each indicator was determined based on the performance disparities between the full model and the sub-models.

$$\text{MAE} = \frac{1}{\text{n}} \sum_{i=1}^{n} |\text{FL}_\text{i} - \text{FO}_\text{i}| \quad (6)$$

Here, FL_i represents the flood value, FO_i signifies the flood output, and n denotes the total number of samples in the training dataset.

3.3. Model Configuration and Training

At the core of the proposed model, we define the 1D-CNN as a pattern recognizer aimed at inferring the twelve flood indicators into flood and non-flood classes. Consequently, the structure of the proposed 1D-CNN model includes an input layer, four 1D-CNN layers, two pooling layers, one flattened layer, two fully connected layers, and an output layer. The activation functions chosen for this model are ReLU for the intermediate layers and Sigmoid for the output layer.

For the first 1D-CNN layer, we employed 32 filters and a kernel size of 1, whereas we used 64 filters and a kernel size of 3 for the second 1D-CNN layer. The third 1D-CNN layer utilized a kernel size of 1 and 64 filters, and the fourth 1D-CNN layer employed a kernel size of 3 and 128 filters. The pool size was 2 for pooling layers 1 and 2. Following the addition of the flattened layer (as illustrated in Figure 5), the architecture included two fully connected layers: the first one with 200 neurons and the second with 50 neurons. Lastly, the output layer was structured with two neurons, each representing "non-flood" and "flood" categories, respectively.

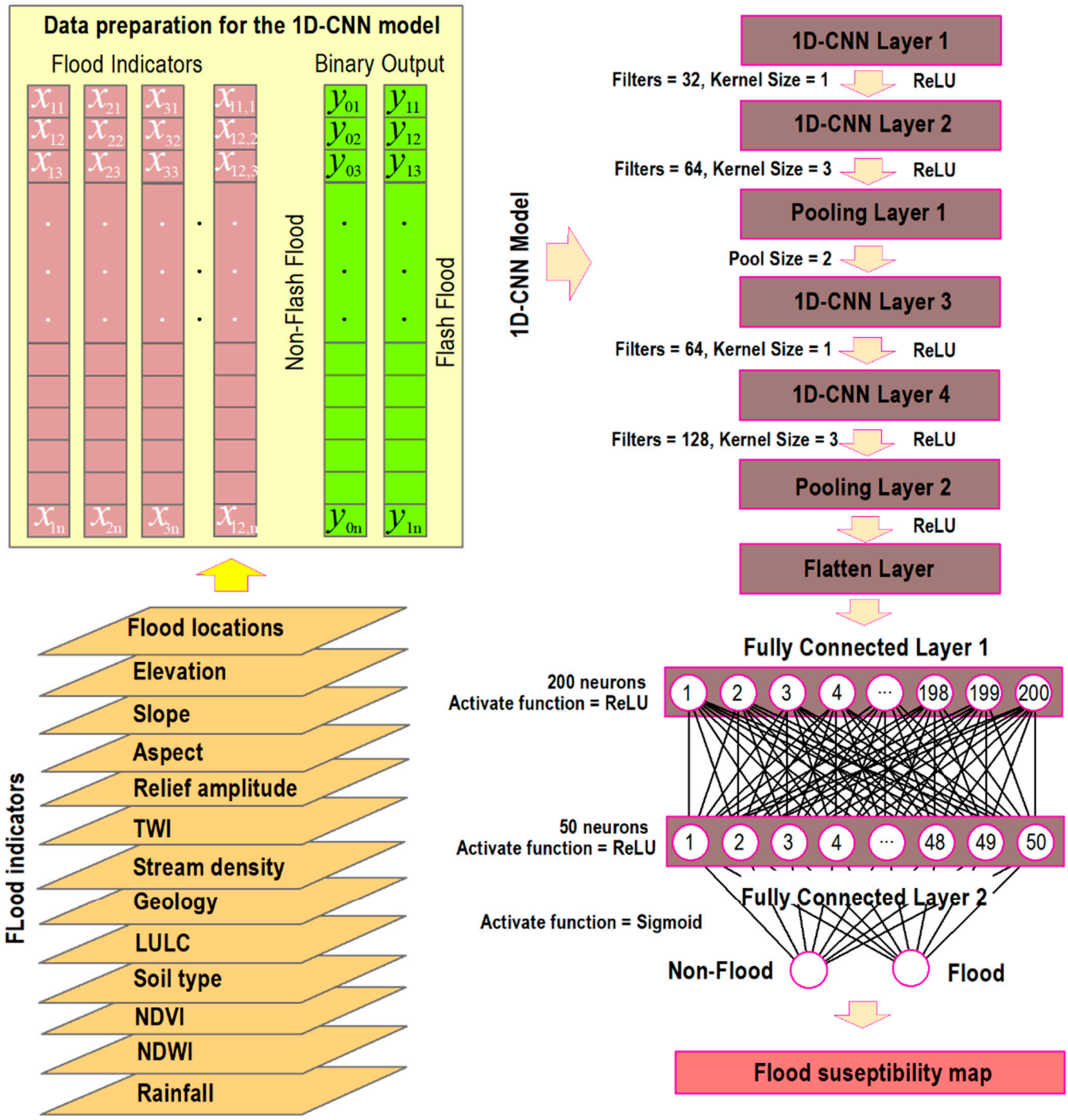

Figure 5. Data and structure of the proposed 1D-CNN model for this research.

Consequently, the proposed 1D-CNN model for fluvial flood modeling was determined to have a total of 71,088 parameters. We chose to optimize the parameters using Adaptive Moment Estimation (ADAM), an algorithm introduced by Kingma and Ba [71], because this algorithm has demonstrated its efficiency in previous flood modeling research [21,28]. Herein, the ADAM algorithm computes the individual learning rates for each parameter in the 1D-CNN model by considering their historical gradients. This adaptiveness significantly enhances the optimizer's efficiency, enabling faster convergence than traditional optimizers with fixed learning rates, as noted by Goodfellow et al. [72].

In the training phase of the 1D-CNN, the 71,088 weights of the model needed to be adapted to establish the optimal functional mapping between the actual and predicted flood and non-flood class labels. To adjust these connecting weights, we utilized the Mean Squared Error (MSE) as a loss function (Equation (7)). MSE was employed for its ability to ensure that the trained model did not have outlier predictions with significant errors. This is because MSE assigns greater importance to errors due to its squaring mechanism [73], meaning that their impact on the model's performance is amplified.

$$\mathrm{MSE} = \frac{1}{\mathrm{n}} \sum_{\mathrm{i}=1}^{\mathrm{n}} (\mathrm{FL_i} - \mathrm{FO_i})^2 \tag{7}$$

where $\mathrm{FL_i}$ represents the flood value, $\mathrm{FO_i}$ signifies the flood output from the 1D-CNN model, and n denotes the total number of samples in the training dataset.

3.4. Model Validation

This study conceptualized the fluvial flood modeling employing 1D-CNN as a pattern recognition task. To comprehensively evaluate the model's performance, various metrics were utilized, i.e., accuracy (Acc), sensitivity (Sens), specificity (Spec), positive predictive value (PPV), negative predictive value (NPV), F-score, Kappa, the Receiver Operating Characteristic (ROC) curve, and the Area Under the Curve (AUC) [74]. These metrics were selected due to their ability to comprehensively evaluate the 1D-CNN model, capturing different facets of its performance.

Accuracy (Acc) signifies the overall correctness of the model's predictions, while sensitivity (Sens) and specificity (Spec) indicate the model's ability to correctly identify flood and non-flood samples, respectively. Positive predictive value (PPV) and negative predictive value (NPV) denote the accuracy of flood and non-flood predictions made by the 1D-CNN model. F-Score represents a balance between PPV and Sens, offering equilibrium between these metrics. Kappa measures the agreement between the observed accuracy and the expected accuracy [75]. Furthermore, the ROC curve and AUC were used to measure the global performance of the 1D-CNN model.

3.5. Benchmark Model Comparison

In this study, to showcase the efficacy of the proposed 1D-CNN model, three benchmark flood models, Deep Neural Network (DeepNN), Support Vector Machine (SVM), and Logistic Regression (LR), were chosen for comparative analysis. In the case of the Deep Neural Network (DeepNN), the model architecture comprised an input layer with 12 neurons, three hidden layers with 64 neurons each, and an output layer with one neuron, following the configuration proposed by Tien Bui, Hoang, Martínez-Álvarez, Ngo, Hoa, Pham, Samui, and Costache [21]. The activation functions chosen for DeepNN were Sigmoid and ReLU for the output and hidden layers, respectively. Consequently, a total of 9217 parameters were identified and subsequently optimized using the ADAM algorithm, employing the Mean Squared Error (MSE) as the loss function. For the SVM, the radial basis function (RBF) kernel was chosen, where two parameters, C and gamma, were determined using the grid search method [76]. Regarding the LR, the default parameters were used.

3.6. Fluvial Flood Susceptibility Map

After successfully training and validating the 1D-CNN model, the model was utilized to generate a fluvial flood susceptibility map for the entire study area. Herein, the probability value of the flood class was used to indicate fluvial flood susceptibility.

4. Result and Analysis

4.1. The Role of the Flood Indicator

The results of the feature selection process for flood indicators are presented in Table 3. It may be seen that all indicators exhibited correlations with fluvial flood occurrences, with LULC showing the highest correlation (0.606), whereas both NDVI and NDWI demonstrated the lowest correlations (0.034) (Table 3). When considering the mutual interactions among these indicators, the result in Table 3 emphasizes the substantial influence of slope, LULC, and rainfall on fluvial floods in the study area. These factors obtained the highest-ranking scores of 0.228, 0.227, and 0.214, respectively. They were followed by soil type (0.190), elevation (0.172), relief amplitude (0.161), geology (0.160), TWI (0.121), stream density (0.079), and aspect (0.017), all of which have been identified as contributors to fluvial flooding. In contrast, NDWI and NDWI exhibited the lowest contribution, with a ranking score of 0.008 (Table 3). Nevertheless, all flood indicators proved to be relevant and informative for fluvial flood analysis. Consequently, all indicators were incorporated into the spatial modeling and prediction of fluvial floods.

Table 3. Evaluating the significance of the twelve flood indicators in this study.

Flood Indicators	Scored Value	Pearson's Correlation	Ranking
Slope (°)	0.228	0.498	1
LULC	0.227	0.606	2
Rainfall (mm)	0.214	0.445	3
Soil type	0.190	0.231	4
Elevation (m)	0.172	0.447	5
Relief amplitude	0.161	0.496	6
Geology	0.160	0.406	7
TWI	0.121	0.375	8
Stream density (km/km^2)	0.079	0.309	9
Aspect	0.017	0.064	10
NDVI	0.008	0.034	11
NDWI	0.008	0.034	12

4.2. Model Training and Validation

By utilizing the training dataset consisting of 5818 samples, the 1D-CNN model was trained, adjusting a total of 71,088 weights that were optimized through the ADAM algorithm. The result is presented in Table 4 and Figure 6a. The result shows that the obtained accuracy (Acc) was 94.3%, the F-score was 0.944, the Kappa value was 0.886, the area under the curve (AUC) was 0.981, and MSE was 0.043, demonstrating a robust correspondence between the trained 1D-CNN model and the training dataset. In addition, the error of the 1D-CNN model followed a normal distribution curve (Figure 6a). The sensitivity (Sens) and specificity (Spec) values stood at 92.0% and 96.8%, indicating the model's ability to accurately discern floods and non-flood events at these rates, respectively. The positive predictive value (PPV) and negative predictive value (NPV) were 97.0% and 91.5%, respectively, signifying the 1D-CNN model's precise classification of floods and non-flood events at these respective percentages.

Table 4. Performance of the flood models using the training dataset.

Flood Model	Performance Metrics											
	TP	TN	FP	FN	PPV (%)	NPV (%)	Sens (%)	Spec (%)	Acc (%)	F-Score	Kappa	AUC
1D-CNN	2822	2663	87	246	97.0	91.5	92.0	96.8	94.3	0.944	0.886	0.981
DeepNN	2672	2639	237	270	91.9	90.7	90.8	91.8	91.3	0.913	0.826	0.966
SVM	2795	2443	114	466	96.1	84.0	85.7	95.5	90.0	0.906	0.801	0.961
LR	2692	1981	217	928	92.5	68.1	74.4	90.1	80.3	0.825	0.606	0.875

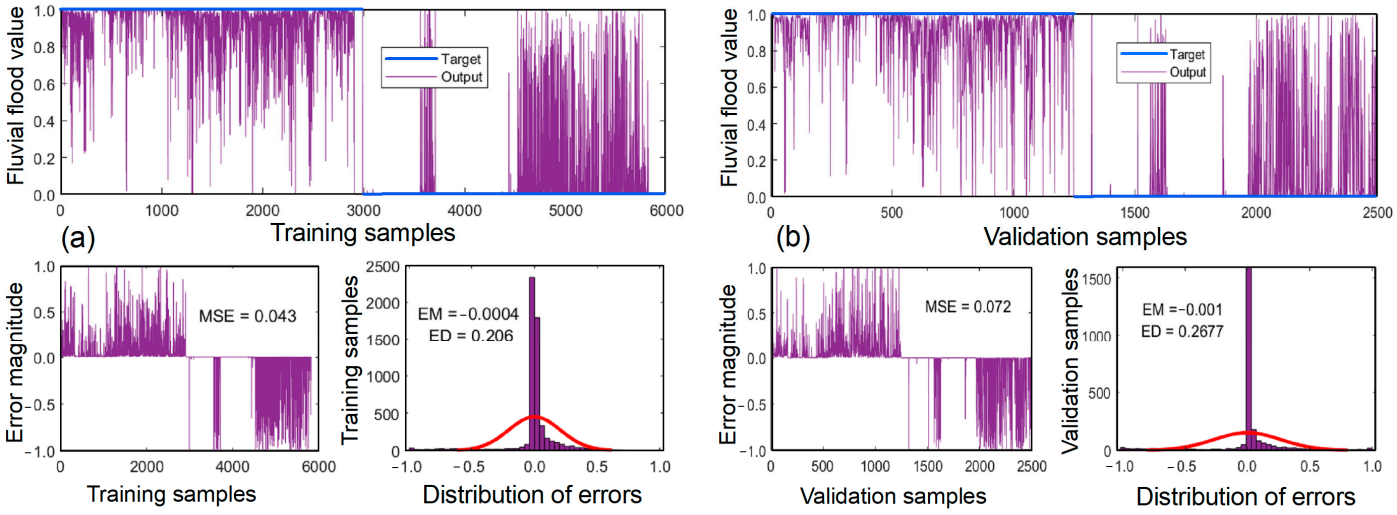

Figure 6. Magnitude and distribution of error of the 1D-CNN model: (**a**) the training dataset and (**b**) the validation dataset.

In order to evaluate the flood model's performance, generalizability, accuracy, and reliability in predicting new data, a validation process was conducted using the validation dataset consisting of 2494 samples. The result is shown in Table 5 and Figure 6b. We observe that the prediction accuracy (Acc) was 90.7%, the F-score was 0.910, the Kappa value was 0.814, and the MSE was 0.072, demonstrating a high prediction performance. The AUC was 0.963, indicating a global prediction performance of 96.3%.

Table 5. Performance of the models using the validation dataset.

Flood Model	Performance Metrics											
	TP	TN	FP	FN	PPV (%)	NPV (%)	Sens (%)	Spec (%)	Acc (%)	F-Score	Kappa	AUC
1D-CNN	1167	1095	80	152	93.6	87.8	88.5	93.2	90.7	0.910	0.814	0.963
DeepNN	1137	1088	110	159	91.2	87.2	87.7	90.8	89.2	0.894	0.784	0.958
SVM	1172	1007	75	240	94.0	80.8	83.0	93.1	87.4	0.882	0.747	0.943
LR	1149	843	98	404	92.1	67.6	74.0	89.6	79.9	0.821	0.597	0.874

The sensitivity (Sens) and specificity (Spec) values were 88.5% and 93.2%, demonstrating the model's accurate prediction of floods and non-flood events at these rates. Moreover, the positive predictive value (PPV) and negative predictive value (NPV) were 93.6% and 87.8%, respectively, indicating the 1D-CNN model's precise classification of floods and non-flood events at these percentages. Additionally, the errors of the 1D-CNN model in the validation dataset were normally distributed, as illustrated in Figure 6b, denoting the reliability of the validation result.

4.3. Model Comparison

As mentioned in Section 3.5, we selected Deep Neural Network (DeepNN), Support Vector Machine (SVM), and Logistic Regression (LR) as benchmarks for a comparative analysis to demonstrate the efficacy of the proposed 1D-CNN model. For the DeepNN, the model was trained and optimized using the ADAM algorithm, whereas for the SVM, Gamma of 0.855 and C of 2000 were found using the grid search. The training results of the DeepNN, SVM, and LR models are shown in Tables 4 and 5. It is evident that the DeepNN model (Acc = 91.3%, Kappa = 0.826, and AUC = 0.966), the SVM model (Acc = 90.0%, Kappa = 0.801, and AUC = 0.961), and the LR model (Acc = 80.3%, Kappa = 0.606, and AUC = 0.875) exhibited excellent performance (Table 4). However, when compared to the proposed 1D-CNN, the performance of these three models was still inferior.

Regarding the prediction result, the DeepNN model (Acc = 89.2%, Kappa = 0.784, and AUC = 0.958) exhibited the highest performance (Table 5). It was followed by the SVM model (Acc = 87.4%, kappa = 0.747, and AUC = 0.943) and the LR model (Acc = 79.9%, kappa = 0.597, and AUC = 0.874). Nevertheless, the prediction performance of all three benchmark models was lower than that of the proposed 1D-CNN (Table 5).

In order to determine if the prediction performance of the proposed 1D-CNN model was statistically higher than those of the three benchmarks, i.e., DeepNN, SVM, and LR, we carried out a paired-sample sign test. This is a non-parametric statistical test which can be valuable for comparing the performance of two models where the data do not adhere to the assumptions of a normal distribution. The null hypothesis (H0) posited no significant difference in prediction performance among the four fluvial flood models, i.e., 1D-CNN, DeepNN, SVM, and LR, at a significance level of $\alpha = 5\%$. The Z-values and *p*-values were computed for each model pair. The null hypothesis was rejected if the *p*-value was less than or equal to 0.05 and the Z-value fell outside the range of −1.96 to +1.96. In such cases, it was concluded that the prediction performance of the 1D-CNN model was statistically superior to the three benchmark models.

The results of the paired-sample sign test are presented in Table 6. It is noteworthy that the p-value was less than 0.05, and the test statistic values for all pairs of flood models (1D-CNN vs. DeepNN, 1D-CNN vs. SVM, 1D-CNN vs. LR, DeepNN vs. SVM, DeepNN vs. LR, and SVM vs. LR) fell outside the critical range of −1.96 to +1.96. This finding signifies that the predictive performance of the proposed 1D-CNN model surpassed that of the three benchmark models, i.e., DeepNN, SVM, and LR.

Table 6. Paired-sample sign test of the 1D-CNN, DeepNN, SVM, and LR models for spatial prediction of fluvial flood.

No.	Pair of the Flood Models	Z-Value	*p*-Value	Significance
1	1D-CNN vs. DeepNN	11.311	<0.001	Yes
2	1D-CNN vs. SVM	11.151	<0.001	Yes
3	1D-CNN vs. LR	6.916	<0.001	Yes
4	DeepNN vs. SVM	8.305	<0.001	Yes
5	DeepNN vs. LR	6.411	<0.001	Yes
6	SVM vs. LR	3.240	0.001	Yes

4.4. Determining Fluvial Flood Susceptibility

As the 1D-CNN model proved to be the most suitable choice for this analysis, the model was employed to calculate Fluvial Flood Susceptibility (FFS) indices for all pixels within the study area. The study area, with a resolution of 30 m, comprised a matrix of 5488 columns × 4105 rows, resulting in the computation of FFS indices for 22,528,240 pixels. The FFS index values ranged from 0.00 to 1.00, representing non-flood to flood conditions. Subsequently, these indices were categorized into three classes: no fluvial flood, low fluvial flood, and high fluvial flood (Figure 7), utilizing the standard deviation method available in ArcGIS Pro. As a result, two threshold values, 0.048 and 0.126, were determined.

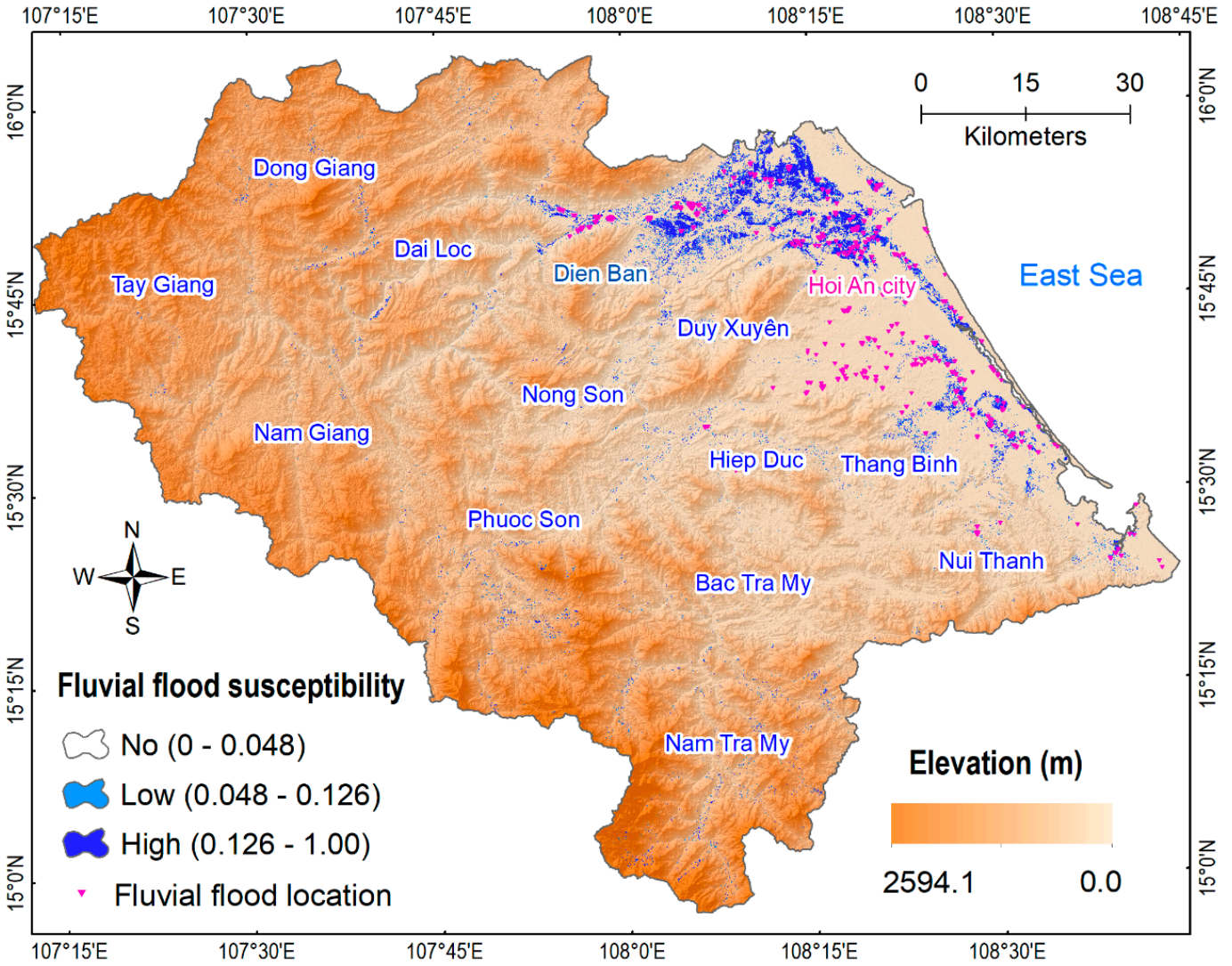

Figure 7. Fluvial flood susceptibility map using the proposed 1D-CNN model for the Quang Nam province.

Aerial interpretation of the map reveals that the province's coastal regions, specifically the Dien Ban, Hoi An, Thang Binh, and Nui Thanh districts (as shown in Figure 7), are the most prone to fluvial flooding. These areas, characterized by flat terrain, have experienced recurrent fluvial flood issues over the last few decades. Conversely, the western parts of the province, which are mountainous with high altitude and steep slopes, are less susceptible to fluvial flooding.

The characteristics of the three fluvial flood susceptibility classes generated by the proposed 1D-CNN model for the study area are presented in Table 7. It may be observed that 165.7 km^2 and 44.1 km^2 of the study area are classified as being of high- and low-risk of fluvial flooding, respectively, constituting 2.00% of the total study area. Conversely, 98.00% of the total study area is classified as having no fluvial flood susceptibility.

Table 7. Characteristics of three fluvial flood susceptibility classes of the proposed 1D-CNN model for Quang Nam province.

No.	FFS Index	Description	Occupied Areas (km^2)	Map (%)
2	0.126–1.000	High fluvial flood	165.7	1.58
3	0.048–0.126	Low fluvial flood	44.1	0.42
5	0.000–0.048	No fluvial flood	10292.5	98.00

5. Discussions

Floods continue to be a global concern [77,78], particularly in the western Pacific region, which is frequently impacted by tropical cyclones characterized by intense and prolonged rainfall [79,80]. While addressing flood challenges demands a multifaceted approach involving sustainable land use practices, improved infrastructure, community education, and comprehensive disaster preparedness and response strategies, accurate flood prediction continues to play a pivotal role. Therefore, this study proposes a new approach based on the 1D-CNN for predicting fluvial floods with a focus on the high-frequency flood province of Quang Nam in Central Vietnam.

The findings in this research indicate that the 1D-CNN model has the ability to capture intricate fluvial flood patterns and dependencies within one-dimensional data sequences. Furthermore, by leveraging the four convolutional layers, two pooling layers, one flattened layer, and two fully connected layers, the 1D-CNN model could effectively analyze spatial variations and relationships in flood data along a single dimension, making it particularly well-suited for tasks where the sequential nature of data is crucial, such as in flood modeling. This unique capability enables the 1D-CNN model to extract meaningful features from spatial data, enhancing its accuracy in predicting and mapping fluvial flood occurrences. As a result, the high prediction performance of the proposed 1D-CNN model indicates that the model's architecture has been meticulously designed. The effectiveness of the ADAM algorithm, coupled with the MSE loss function, was reaffirmed by optimizing the 71,088 model weights. Nevertheless, asserting that this represents the optimal structure of a 1D-CNN model for the study area is challenging. Therefore, further research is necessary to refine the 1D-CNN model's structure, specifically for spatial predictions of fluvial floods. This entails automating the process to tailor the model's architecture for various study areas, thereby increasing its applicability to regions with diverse geo-environmental conditions.

When comparing the proposed 1D-CNN model with three benchmarks (DeepNN, SVM, and LR), the findings demonstrate its superior performance, as confirmed by the paired-sample sign test. This underscores the potential of 1D-CNN as a promising tool for spatial predictions of fluvial floods. These findings align with existing literature [24–26,81], emphasizing the efficacy of novel deep learning approaches in achieving superior prediction accuracy in flood studies, surpassing traditional machine learning models. Herein, the 1D-CNN model performs better than the DeepNN because the fluvial flood patterns in the study area are local, meaning they depend on nearby data points. Thus, the 1D-CNN uses local receptive fields [82], allowing it to focus on specific regions of input data, which is particularly effective for capturing local fluvial flood patterns compared to the DeepNN. Moreover, the 1D-CNN exhibits reduced sensitivity to minor spatial fluctuations [83], enabling it to recognize spatial patterns even when their precise locations within the input data differ slightly. In the context of fluvial flood prediction, where the exact locations of potential flood events might not always be accurately determined, this ability to tolerate spatial variance proves to be highly beneficial. In this study, the 1D-CNN model outperformed SVM and LR due to its capability to capture intricate fluvial flood patterns while emphasizing local contexts. Consequently, the 1D-CNN model adapted better to the complexity of the fluvial flood data. In terms of computational resources, the 1D-CNN model was trained on a Dell desktop computer equipped with x64-based processing, 32 GB of installed RAM, an Intel Core i7-3800 CPU running at 3.20 GHz, and an NVIDIA GPU. Impressively, the training process of both 1D-CNN and DeepNN was completed in less than one minute, highlighting its computational efficiency.

In this analysis, all twelve indicators were meticulously selected through a comprehensive review of existing literature, an in-depth analysis of the characteristics of the study area, and the availability of relevant data. However, it is essential to explore and consider additional indicators for future flood modeling endeavors. Nevertheless, all indicators provided valuable information for fluvial flood modeling, contributing to the excellent prediction performance of the 1D-CNN model. Consequently, it can be concluded that the selection, processing, and encoding of these indicators were conducted successfully.

Among them, slope, LULC, and rainfall were found to be the most critical factors. This is a reasonable result, because the fluvial floods in the study area are mainly concentrated in gentler slopes and flat areas (i.e., Dien Ba, Hoi An, Thang Binh, and Nui Thanh, as shown in Figure 7), which decelerates the velocity of flow and causes flooding. For the LULC, the rapid urbanization and industrialization in the province over the last two decades, as documented by Nguyen, et al. [84], have resulted in significant changes in LULC. These changes have led to the covering of natural waterways and drainage systems, causing floods. Rainfall also serves as a critical indicator; Quang Nam Province experiences some of the heaviest rainfall in Vietnam [29], and tropical storms, often accompanied by intense rainfall, lead to annual flooding in this area [85,86].

Limitations of the applied data stem from differences in resolutions among the sources. Specifically, DEM and its derivatives (NDVI and NDWI) have a spatial resolution of 30 m. In contrast, the soil map was derived from national pedology maps at a 1:100,000 scale, and the geology data originated from Geological and Mineral Resources Maps at a scale of 1:200,000. Consequently, there may be discrepancies in content and accuracy across the original maps, leading to uncertainties in the flood model. Additionally, the 12-component and status maps were processed and extracted from eight different data sources, making it challenging to eliminate inconsistencies in the final maps. As a result, the flood susceptibility map generated in this study is most suitable for a provincial scale. To enhance forecast accuracy, it is imperative to collect data at higher resolutions, such as through the use of UAVs or LiDAR technology [87].

Nevertheless, the fluvial flood susceptibility modeling in this research holds significant implications, extending to its potential applications in flood risk management and policy formulation. Thus, the susceptibility map could be an important input for flood risk assessment. Furthermore, by understanding the indicators contributing to fluvial flood susceptibility, authorities can develop informed strategies for mitigating risks, enhancing disaster preparedness, and formulating policies that promote resilient communities and infrastructure.

6. Conclusions

In this research, we introduced and validated a novel modeling approach that utilizes 1D-CNN and geospatial data for spatial predictions of fluvial floods. Based on the findings presented, we have reached the following conclusions:

- 1D-CNN with the ADAM optimizer and the MSE loss function is capable of producing fluvial flood susceptibility maps with high accuracy.
- The performance of the proposed 1D-CNN model surpassed that of the DeepNN, SVM, and LR models, which were used for benchmarking. This outcome suggests that 1D-CNN stands as a promising and innovative tool for susceptibility mapping of fluvial floods.
- Slope, LULC, and rainfall were found to be the most critical factors for fluvial floods in this study area.
- The fluvial flood susceptibility map generated by the 1D-CNN model in this study holds significant potential to provide a valuable tool to policymakers and authorities in Quang Nam Province, aiding in the implementation of effective flood hazard management practices.
- Future research should concentrate on the temporal prediction of fluvial floods and risk assessment, as well as the development of frameworks for issuing warnings and delivering flood predictions to the community.

Author Contributions: Conceptualization: N.G.T., P.N.Q., N.V.C., H.A.L., H.L.N. and D.T.B.; methodology: N.G.T., P.N.Q., N.V.C., H.A.L., H.L.N. and D.T.B.; validation, N.G.T., P.N.Q., H.L.N. and D.T.B.; writing-original draft preparation: N.G.T., P.N.Q., N.V.C., H.A.L., H.L.N. and D.T.B.; writing-review and editing: N.G.T. and D.T.B. All authors have read and agreed to the published version of the manuscript.

Funding: This work was financially supported by the Ministry of Natural Research and Environment in Vietnam under grant number TNMT.2022.04.09.

Data Availability Statement: The data presented in this study are available on request from the first author. The data are not publicly available due to privacy.

Conflicts of Interest: The authors declare no conflict of interest.

References

1. Wallemacq, P.; Below, R.; McLean, D. *UNISDR and CRED Report: Economic Losses, Poverty & Disasters (1998–2017)*; CRED: Brussels, Belgium, 2018.
2. Boulange, J.; Hanasaki, N.; Yamazaki, D.; Pokhrel, Y. Role of dams in reducing global flood exposure under climate change. *Nat. Commun.* **2021**, *12*, 417. [CrossRef] [PubMed]
3. Devitt, L.; Neal, J.; Coxon, G.; Savage, J.; Wagener, T. Flood hazard potential reveals global floodplain settlement patterns. *Nat. Commun.* **2023**, *14*, 2801. [CrossRef] [PubMed]
4. Alifu, H.; Hirabayashi, Y.; Imada, Y.; Shiogama, H. Enhancement of river flooding due to global warming. *Sci. Rep.* **2022**, *12*, 20687. [CrossRef]
5. Viglione, A.; Rogger, M. Chapter 1—Flood Processes and Hazards. In *Hydro-Meteorological Hazards, Risks and Disasters*; Shroder, J.F., Paron, P., Baldassarre, G.D., Eds.; Elsevier: Boston, MA, USA, 2015; pp. 3–33.
6. Rentschler, J.; Salhab, M.; Jafino, B.A. Flood exposure and poverty in 188 countries. *Nat. Commun.* **2022**, *13*, 3527. [CrossRef]
7. Mudashiru, R.B.; Sabtu, N.; Abustan, I.; Balogun, W. Flood hazard mapping methods: A review. *J. Hydrol.* **2021**, *603*, 126846. [CrossRef]
8. Lavtar, K.; Bezak, N.; Šraj, M. Rainfall-Runoff Modeling of the Nested Non-Homogeneous Sava River Sub-Catchments in Slovenia. *Water* **2019**, *12*, 128. [CrossRef]
9. Tien Bui, D.; Pradhan, B.; Nampak, H.; Bui, Q.-T.; Tran, Q.-A.; Nguyen, Q.-P. Hybrid artificial intelligence approach based on neural fuzzy inference model and metaheuristic optimization for flood susceptibilitgy modeling in a high-frequency tropical cyclone area using GIS. *J. Hydrol.* **2016**, *540*, 317–330. [CrossRef]
10. Ponce, V.M.; Hawkins, R.H. Runoff Curve Number: Has It Reached Maturity? *J. Hydrol. Eng.* **1996**, *1*, 11–19. [CrossRef]
11. Vincendon, B.; Ducrocq, V.; Saulnier, G.-M.; Bouilloud, L.; Chancibault, K.; Habets, F.; Noilhan, J. Benefit of coupling the ISBA land surface model with a TOPMODEL hydrological model version dedicated to Mediterranean flash-floods. *J. Hydrol.* **2010**, *394*, 256–266. [CrossRef]
12. Jodar-Abellan, A.; Valdes-Abellan, J.; Pla, C.; Gomariz-Castillo, F. Impact of land use changes on flash flood prediction using a sub-daily SWAT model in five Mediterranean ungauged watersheds (SE Spain). *Sci. Total Environ.* **2019**, *657*, 1578–1591. [CrossRef]
13. Yu, S.; Bond, N.R.; Bunn, S.E.; Xu, Z.; Kennard, M.J. Quantifying spatial and temporal patterns of flow intermittency using spatially contiguous runoff data. *J. Hydrol.* **2018**, *559*, 861–872. [CrossRef]
14. Tien Bui, D.; Hoang, N.-D. A Bayesian framework based on a Gaussian mixture model and radial-basis-function Fisher discriminant analysis (BayGmmKda V1.1) for spatial prediction of floods. *Geosci. Model Dev.* **2017**, *10*, 3391–3409. [CrossRef]
15. Choubin, B.; Moradi, E.; Golshan, M.; Adamowski, J.; Sajedi-Hosseini, F.; Mosavi, A. An ensemble prediction of flood susceptibility using multivariate discriminant analysis, classification and regression trees, and support vector machines. *Sci. Total Environ.* **2019**, *651*, 2087–2096. [CrossRef]
16. Wang, Z.; Lai, C.; Chen, X.; Yang, B.; Zhao, S.; Bai, X. Flood hazard risk assessment model based on random forest. *J. Hydrol.* **2015**, *527*, 1130–1141. [CrossRef]
17. Khosravi, K.; Pham, B.T.; Chapi, K.; Shirzadi, A.; Shahabi, H.; Revhaug, I.; Prakash, I.; Tien Bui, D. A comparative assessment of decision trees algorithms for flash flood susceptibility modeling at Haraz watershed, northern Iran. *Sci. Total Environ.* **2018**, *627*, 744–755. [CrossRef]
18. Ngo, P.-T.T.; Hoang, N.-D.; Pradhan, B.; Nguyen, Q.K.; Tran, X.T.; Nguyen, Q.M.; Nguyen, V.N.; Samui, P.; Tien Bui, D. A Novel Hybrid Swarm Optimized Multilayer Neural Network for Spatial Prediction of Flash Floods in Tropical Areas Using Sentinel-1 SAR Imagery and Geospatial Data. *Sensors* **2018**, *18*, 3704. [CrossRef]
19. Hong, H.; Panahi, M.; Shirzadi, A.; Ma, T.; Liu, J.; Zhu, A.X.; Chen, W.; Kougias, I.; Kazakis, N. Flood susceptibility assessment in Hengfeng area coupling adaptive neuro-fuzzy inference system with genetic algorithm and differential evolution. *Sci. Total Environ.* **2018**, *621*, 1124–1141. [CrossRef]
20. Bui, D.T.; Hoang, N.-D.; Pham, T.-D.; Ngo, P.-T.T.; Hoa, P.V.; Minh, N.Q.; Tran, X.-T.; Samui, P. A new intelligence approach based on GIS-based Multivariate Adaptive Regression Splines and metaheuristic optimization for predicting flash flood susceptible areas at high-frequency tropical typhoon area. *J. Hydrol.* **2019**, *575*, 314–326. [CrossRef]
21. Bui, D.T.; Hoang, N.-D.; Martínez-Álvarez, F.; Ngo, P.-T.T.; Hoa, P.V.; Pham, T.D.; Samui, P.; Costache, R. A novel deep learning neural network approach for predicting flash flood susceptibility: A case study at a high frequency tropical storm area. *Sci. Total Environ.* **2020**, *701*, 134413. [CrossRef]
22. Kalantar, B.; Ueda, N.; Saeidi, V.; Janizadeh, S.; Shabani, F.; Ahmadi, K.; Shabani, F. Deep neural network utilizing remote sensing datasets for flood hazard susceptibility mapping in Brisbane, Australia. *Remote Sens.* **2021**, *13*, 2638. [CrossRef]

23. Fang, Z.; Wang, Y.; Peng, L.; Hong, H. Predicting flood susceptibility using LSTM neural networks. *J. Hydrol.* **2021**, *594*, 125734. [CrossRef]
24. Tsangaratos, P.; Ilia, I.; Chrysafi, A.-A.; Matiatos, I.; Chen, W.; Hong, H. Applying a 1D Convolutional Neural Network in Flood Susceptibility Assessments—The Case of the Island of Euboea, Greece. *Remote Sens.* **2023**, *15*, 3471. [CrossRef]
25. Wang, Y.; Fang, Z.; Hong, H.; Peng, L. Flood susceptibility mapping using convolutional neural network frameworks. *J. Hydrol.* **2020**, *582*, 124482. [CrossRef]
26. Pradhan, B.; Lee, S.; Dikshit, A.; Kim, H. Spatial flood susceptibility mapping using an explainable artificial intelligence (XAI) model. *Geosci. Front.* **2023**, *14*, 101625. [CrossRef]
27. Vincent, A.M.; Parthasarathy, K.S.S.; Jidesh, P. Flood susceptibility mapping using AutoML and a deep learning framework with evolutionary algorithms for hyperparameter optimization. *Appl. Soft Comput.* **2023**, *148*, 110846. [CrossRef]
28. Melgar-García, L.; Martínez-Álvarez, F.; Tien Bui, D.; Troncoso, A. A novel semantic segmentation approach based on U-Net, WU-Net, and U-Net++ deep learning for predicting areas sensitive to pluvial flood at tropical area. *Int. J. Digit. Earth* **2023**, *16*, 3661–3679. [CrossRef]
29. Tuan, T.A.; Pha, P.D.; Tam, T.T.; Bui, D.T. A new approach based on Balancing Composite Motion Optimization and Deep Neural Networks for spatial prediction of landslides at tropical cyclone areas. *IEEE Access* **2023**, *11*, 69495–69511. [CrossRef]
30. Lepvrier, C.; Maluski, H.; Van Tich, V.; Leyreloup, A.; Thi, P.T.; Van Vuong, N. The early Triassic Indosinian orogeny in Vietnam (Truong Son Belt and Kontum Massif); implications for the geodynamic evolution of Indochina. *Tectonophysics* **2004**, *393*, 87–118. [CrossRef]
31. Tra, T.V.; Thinh, N.X.; Greiving, S. Combined top-down and bottom-up climate change impact assessment for the hydrological system in the Vu Gia- Thu Bon River Basin. *Sci. Total Environ.* **2018**, *630*, 718–727. [CrossRef]
32. Phuong, D.N.D.; Duong, T.Q.; Liem, N.D.; Tram, V.N.Q.; Cuong, D.K.; Loi, N.K. Projections of future climate change in the Vu Gia Thu Bon River Basin, Vietnam by using statistical downscaling model (SDSM). *Water* **2020**, *12*, 755. [CrossRef]
33. Shrestha, S.; Trang, B.T.T. Assessment of the climate-change impacts and evaluation of adaptation measures for paddy productivity in Quang Nam province, Vietnam. *Paddy Water Environ.* **2015**, *13*, 241–253. [CrossRef]
34. Le, N.T.; Tham, N. Assessing bioclimatic resources for tourism development in Quang Nam province. *J. Sci. Educ.* **2016**, *45*, 159–168.
35. Clement, M.A.; Kilsby, C.; Moore, P. Multi-temporal synthetic aperture radar flood mapping using change detection. *J. Flood Risk Manag.* **2018**, *11*, 152–168. [CrossRef]
36. Amitrano, D.; Di Martino, G.; Iodice, A.; Riccio, D.; Ruello, G. Unsupervised rapid flood mapping using Sentinel-1 GRD SAR images. *IEEE Trans. Geosci. Remote Sens.* **2018**, *56*, 3290–3299. [CrossRef]
37. Pham, B.T.; Luu, C.; Phong, T.V.; Nguyen, H.D.; Le, H.V.; Tran, T.Q.; Ta, H.T.; Prakash, I. Flood risk assessment using hybrid artificial intelligence models integrated with multi-criteria decision analysis in Quang Nam Province, Vietnam. *J. Hydrol.* **2021**, *592*, 125815. [CrossRef]
38. Bui, D.T.; Ngo, P.-T.T.; Pham, T.D.; Jaafari, A.; Minh, N.Q.; Hoa, P.V.; Samui, P. A novel hybrid approach based on a swarm intelligence optimized extreme learning machine for flash flood susceptibility mapping. *Catena* **2019**, *179*, 184–196. [CrossRef]
39. Ngo, P.-T.T.; Pham, T.D.; Hoang, N.-D.; Tran, D.A.; Amiri, M.; Le, T.T.; Hoa, P.V.; Van Bui, P.; Nhu, V.-H.; Bui, D.T. A new hybrid equilibrium optimized SysFor based geospatial data mining for tropical storm-induced flash flood susceptible mapping. *J. Environ. Manag.* **2021**, *280*, 111858. [CrossRef]
40. Chapi, K.; Singh, V.P.; Shirzadi, A.; Shahabi, H.; Bui, D.T.; Pham, B.T.; Khosravi, K. A novel hybrid artificial intelligence approach for flood susceptibility assessment. *Environ. Model. Softw.* **2017**, *95*, 229–245. [CrossRef]
41. Tehrany, M.S.; Pradhan, B.; Mansor, S.; Ahmad, N. Flood susceptibility assessment using GIS-based support vector machine model with different kernel types. *Catena* **2015**, *125*, 91–101. [CrossRef]
42. Maidment, D.R. *Arc Hydro: GIS for Water Resources*; ESRI, Inc.: Redlands, CA, USA, 2002.
43. Li, X.; Gao, J.; Guo, Z.; Yin, Y.; Zhang, X.; Sun, P.; Gao, Z. A Study of Rainfall-Runoff Movement Process on High and Steep Slopes Affected by Double Turbulence Sources. *Sci. Rep.* **2020**, *10*, 9001. [CrossRef]
44. Fang, H.; Sun, L.; Tang, Z. Effects of rainfall and slope on runoff, soil erosion and rill development: An experimental study using two loess soils. *Hydrol. Process.* **2015**, *29*, 2649–2658. [CrossRef]
45. García-Ruiz, J.M.; Regüés, D.; Alvera, B.; Lana-Renault, N.; Serrano-Muela, P.; Nadal-Romero, E.; Navas, A.; Latron, J.; Martí-Bono, C.; Arnáez, J. Flood generation and sediment transport in experimental catchments affected by land use changes in the central Pyrenees. *J. Hydrol.* **2008**, *356*, 245–260. [CrossRef]
46. Best, J.; Bridge, J. The morphology and dynamics of low amplitude bedwaves upon upper stage plane beds and the preservation of planar laminae. *Sedimentology* **1992**, *39*, 737–752. [CrossRef]
47. Buchanan, B.; Fleming, M.; Schneider, R.; Richards, B.; Archibald, J.; Qiu, Z.; Walter, M. Evaluating topographic wetness indices across central New York agricultural landscapes. *Hydrol. Earth Syst. Sci.* **2014**, *18*, 3279–3299. [CrossRef]
48. Pallard, B.; Castellarin, A.; Montanari, A. A look at the links between drainage density and flood statistics. *Hydrol. Earth Syst. Sci.* **2009**, *13*, 1019–1029. [CrossRef]
49. Montgomery, D.R.; Buffington, J.M. Channel-reach morphology in mountain drainage basins. *Geol. Soc. Am. Bull.* **1997**, *109*, 596–611. [CrossRef]

50. Mahala, A. The significance of morphometric analysis to understand the hydrological and morphological characteristics in two different morpho-climatic settings. *Appl. Water Sci.* **2020**, *10*, 33. [CrossRef]
51. Van Trang, N. *Geology and Mineral Resources Map of Vietnam Scale 1:200,000, Hue-Quang Ngai Sheet Series*; Department of Geology and Minerals of Vietnam: Hanoi, Vietnam, 1986.
52. Nie, W.; Yuan, Y.; Kepner, W.; Nash, M.S.; Jackson, M.; Erickson, C. Assessing impacts of Landuse and Landcover changes on hydrology for the upper San Pedro watershed. *J. Hydrol.* **2011**, *407*, 105–114. [CrossRef]
53. Kirkby, M.; Bracken, L.; Reaney, S. The influence of land use, soils and topography on the delivery of hillslope runoff to channels in SE Spain. *Earth Surf. Process. Landf. J. Br. Geomorphol. Res. Group* **2002**, *27*, 1459–1473. [CrossRef]
54. Zhan, T.L.; Ng, C.W. Analytical analysis of rainfall infiltration mechanism in unsaturated soils. *Int. J. Geomech.* **2004**, *4*, 273–284. [CrossRef]
55. Mialhe, F.; Gunnell, Y.; Mering, C. Synoptic assessment of water resource variability in reservoirs by remote sensing: General approach and application to the runoff harvesting systems of south India. *Water Resour. Res.* **2008**, 44. [CrossRef]
56. Serrano, L.; Ustin, S.L.; Roberts, D.A.; Gamon, J.A.; Penuelas, J. Deriving water content of chaparral vegetation from AVIRIS data. *Remote Sens. Environ.* **2000**, *74*, 570–581. [CrossRef]
57. Defries, R.S.; Townshend, J.R.G. NDVI-derived land cover classifications at a global scale. *Int. J. Remote Sens.* **1994**, *15*, 3567–3586. [CrossRef]
58. Xu, H. Modification of normalised difference water index (NDWI) to enhance open water features in remotely sensed imagery. *Int. J. Remote Sens.* **2006**, *27*, 3025–3033. [CrossRef]
59. Arthington, A.H. *Environmental Flows: Saving Rivers in the Third Millennium*; University of California Press: Berkeley, CA, USA, 2012; Volume 4.
60. Bui, D.T.; Lofman, O.; Revhaug, I.; Dick, O. Landslide susceptibility analysis in the Hoa Binh province of Vietnam using statistical index and logistic regression. *Nat. Hazards* **2011**, *59*, 1413–1444. [CrossRef]
61. Abedi, R.; Costache, R.; Shafizadeh-Moghadam, H.; Pham, Q.B. Flash-flood susceptibility mapping based on XGBoost, random forest and boosted regression trees. *Geocarto Int.* **2022**, *37*, 5479–5496. [CrossRef]
62. Qu, N.; Li, Z.; Li, X.; Zhang, S.; Zheng, T. Multi-parameter fire detection method based on feature depth extraction and stacking ensemble learning model. *Fire Saf. J.* **2022**, *128*, 103541. [CrossRef]
63. Nava, L.; Carraro, E.; Reyes-Carmona, C.; Puliero, S.; Bhuyan, K.; Rosi, A.; Monserrat, O.; Floris, M.; Meena, S.R.; Galve, J.P. Landslide displacement forecasting using deep learning and monitoring data across selected sites. *Landslides* **2023**, *20*, 2111–2129. [CrossRef]
64. Kiranyaz, S.; Avci, O.; Abdeljaber, O.; Ince, T.; Gabbouj, M.; Inman, D.J. 1D convolutional neural networks and applications: A survey. *Mech. Syst. Signal Process.* **2021**, *151*, 107398. [CrossRef]
65. Zeiler, M. *Modeling Our World: The ESRI Guide to Geodatabase Design*; ESRI, Inc.: Redlands, CA, USA, 1999.
66. Dodangeh, E.; Panahi, M.; Rezaie, F.; Lee, S.; Bui, D.T.; Lee, C.-W.; Pradhan, B. Novel hybrid intelligence models for flood-susceptibility prediction: Meta optimization of the GMDH and SVR models with the genetic algorithm and harmony search. *J. Hydrol.* **2020**, *590*, 125423. [CrossRef]
67. Tehrany, M.S.; Jones, S.; Shabani, F. Identifying the essential flood conditioning factors for flood prone area mapping using machine learning techniques. *CATENA* **2019**, *175*, 174–192. [CrossRef]
68. Pudjihartono, N.; Fadason, T.; Kempa-Liehr, A.W.; O'Sullivan, J.M. A review of feature selection methods for machine learning-based disease risk prediction. *Front. Bioinform.* **2022**, *2*, 927312. [CrossRef] [PubMed]
69. Ngo, P.-T.T.; Pham, T.D.; Nhu, V.-H.; Le, T.T.; Tran, D.A.; Phan, D.C.; Hoa, P.V.; Amaro-Mellado, J.L.; Bui, D.T. A novel hybrid quantum-PSO and credal decision tree ensemble for tropical cyclone induced flash flood susceptibility mapping with geospatial data. *J. Hydrol.* **2021**, *596*, 125682. [CrossRef]
70. Gokalp, O.; Tasci, E.; Ugur, A. A novel wrapper feature selection algorithm based on iterated greedy metaheuristic for sentiment classification. *Expert Syst. Appl.* **2020**, *146*, 113176. [CrossRef]
71. Kingma, D.; Ba, J. Adam: A method for stochastic optimization. In Proceedings of the 3rd international conference for learning representations (iclr'15), San Diego, CA, USA, 7–9 May 2015; Volume 500.
72. Goodfellow, I.; Bengio, Y.; Courville, A. *Deep Learning*; MIT Press: Cambridge, MA, USA, 2016.
73. Elliott, G.; Timmermann, A. Optimal forecast combinations under general loss functions and forecast error distributions. *J. Econom.* **2004**, *122*, 47–79. [CrossRef]
74. Nhu, V.-H.; Thi Ngo, P.-T.; Pham, T.D.; Dou, J.; Song, X.; Hoang, N.-D.; Tran, D.A.; Cao, D.P.; Aydilek, İ.B.; Amiri, M.; et al. A New Hybrid Firefly–PSO Optimized Random Subspace Tree Intelligence for Torrential Rainfall-Induced Flash Flood Susceptible Mapping. *Remote Sens.* **2020**, *12*, 2688. [CrossRef]
75. McHugh, M.L. Interrater reliability: The kappa statistic. *Biochem. Med.* **2012**, *22*, 276–282. [CrossRef]
76. Tehrany, M.S.; Pradhan, B.; Jebur, M.N. Flood susceptibility mapping using a novel ensemble weights-of-evidence and support vector machine models in GIS. *J. Hydrol.* **2014**, *512*, 332–343. [CrossRef]
77. Kautz, L.-A.; Martius, O.; Pfahl, S.; Pinto, J.G.; Ramos, A.M.; Sousa, P.M.; Woollings, T. Atmospheric blocking and weather extremes over the Euro-Atlantic sector–a review. *Weather Clim. Dyn.* **2022**, *3*, 305–336. [CrossRef]
78. Payne, A.E.; Demory, M.-E.; Leung, L.R.; Ramos, A.M.; Shields, C.A.; Rutz, J.J.; Siler, N.; Villarini, G.; Hall, A.; Ralph, F.M. Responses and impacts of atmospheric rivers to climate change. *Nat. Rev. Earth Environ.* **2020**, *1*, 143–157. [CrossRef]

79. Macalalad, R.V.; Badilla, R.A.; Cabrera, O.C.; Bagtasa, G. Hydrological response of the Pampanga River basin in the Philippines to intense tropical cyclone rainfall. *J. Hydrometeorol.* **2021**, *22*, 781–794. [CrossRef]
80. Mirones, Ó.; Bedia, J.; Fernández-Granja, J.A.; Herrera, S.; Van Vloten, S.O.; Pozo, A.; Cagigal, L.; Méndez, F.J. Weather-type-conditioned calibration of Tropical Rainfall Measuring Mission precipitation over the South Pacific Convergence Zone. *Int. J. Climatol.* **2023**, *43*, 1193–1210. [CrossRef]
81. Sameen, M.I.; Pradhan, B.; Lee, S. Application of convolutional neural networks featuring Bayesian optimization for landslide susceptibility assessment. *Catena* **2020**, *186*, 104249. [CrossRef]
82. Wang, X.; Li, R.; Wang, J.; Lei, L.; Song, Y. One-dimension hierarchical local receptive fields based extreme learning machine for radar target HRRP recognition. *Neurocomputing* **2020**, *418*, 314–325. [CrossRef]
83. Du, R.; Zhu, S.; Ni, H.; Mao, T.; Li, J.; Wei, R. Valence-arousal classification of emotion evoked by Chinese ancient-style music using 1D-CNN-BiLSTM model on EEG signals for college students. *Multimed. Tools Appl.* **2023**, *82*, 15439–15456. [CrossRef] [PubMed]
84. Nguyen, B.Q.; Tran, T.-N.-D.; Grodzka-Łukaszewska, M.; Sinicyn, G.; Lakshmi, V. Assessment of urbanization-induced land-use change and its impact on temperature, evaporation, and humidity in central Vietnam. *Water* **2022**, *14*, 3367. [CrossRef]
85. Luu, C.; Von Meding, J.; Kanjanabootra, S. Assessing flood hazard using flood marks and analytic hierarchy process approach: A case study for the 2013 flood event in Quang Nam, Vietnam. *Nat. Hazards* **2018**, *90*, 1031–1050. [CrossRef]
86. Nguyen, B.Q.; Kantoush, S.; Binh, D.V.; Saber, M.; Vo, D.N.; Sumi, T. Understanding the anthropogenic development impacts on long-term flow regimes in a tropical river basin, Central Vietnam. *Hydrol. Sci. J.* **2023**, *68*, 341–354. [CrossRef]
87. Iqbal, A.; Mondal, M.S.; Veerbeek, W.; Khan, M.S.A.; Hakvoort, H. Effectiveness of UAV-based DTM and satellite-based DEMs for local-level flood modeling in Jamuna floodplain. *J. Flood Risk Manag.* **2023**, *16*, e12937. [CrossRef]